AD-A165 805 RADIO PHASE MEASUREMENTS VIA ACOUSTO-OPTICS AND A MACH-ZEHNDER INTERFEROMETER(U) ELECTRONICS RESEARCH LAB ADELAIDE (AUSTRALIA) I G FUSS OCT 84 ERL-0319-TR 1/1

UNCLASSIFIED F/G 20/14 NL

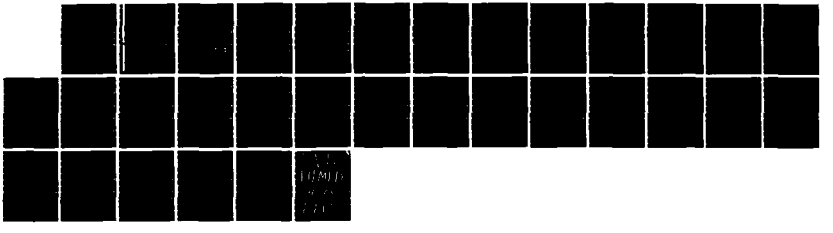

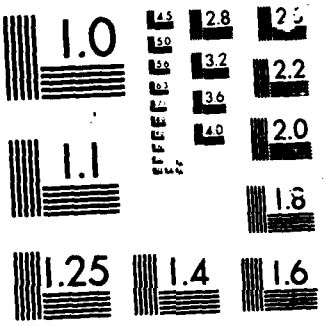

MICROCOPY RESOLUTION TEST CHART

(12)

ERL-0319-TR

AR-004-113

DEPARTMENT OF DEFENCE

DEFENCE SCIENCE AND TECHNOLOGY ORGANISATION

ELECTRONICS RESEARCH LABORATORY

DEFENCE RESEARCH CENTRE SALISBURY
SOUTH AUSTRALIA

TECHNICAL REPORT

ERL-0319-TR

RADIO PHASE MEASUREMENTS VIA ACOUSTO-OPTICS AND A MACH-ZEHNDER INTERFEROMETER

I.G. FUSS

Approved for Public Release

COPY No. 9

OCTOBER 1984

AR-004-113

DEPARTMENT OF DEFENCE

DEFENCE SCIENCE AND TECHNOLOGY ORGANISATION

ELECTRONICS RESEARCH LABORATORY

TECHNICAL REPORT

ERL-039-TR

RADIO PHASE MEASUREMENTS VIA ACOUSTO-OPTICS AND A MACH-ZEHNDER INTERFEROMETER

I.G. Fuss

SUMMARY

A method for simultaneously measuring the frequency spectra of two radio signals, and their relative phase as a function of frequency is described. Measurements made using a prototype verify aspects of this method.

POSTAL ADDRESS: Director, Electronics Research Laboratory,
Box 2151, GPO, Adelaide, South Australia, 5001.

TABLE OF CONTENTS

		Page
1.	INTRODUCTION	1
2.	THE MACH-ZEHNDER ACOUSTO-OPTIC INTERFEROMETER	1
	2.1 Basic optical layout	1
	2.2 Fourier optics and the transmission function for Bragg diffraction	2
	2.3 The Fourier transform configuration	5
	2.4 Determination of optical phase differences from intensities	5
	2.5 Simultaneous radio phase and frequency measurements	6
	2.6 Comparison with the Young's interferometer configuration	7
3.	EXPERIMENTAL STUDIES OF THE MACH-ZEHNDER ACOUSTO-OPTIC INTERFEROMETER	7
	3.1 The optical system	7
	3.2 Alignment of the interferometer	8
	3.3 Wave front distortion of the Bragg cells	8
	3.4 Radio frequency electronics	9
	3.5 Measurements of the Radio Phase Difference	9
4.	CONCLUSIONS	10
5.	ACKNOWLEDGEMENTS	11
	REFERENCES	12

LIST OF FIGURES

1.	This is a Schematic diagram of the optics of the Mach Zehnder acousto-optic interferometer. The labels M0 and M3 denote 50% reflecting mirrors, and M1 and M2 denote 90% reflecting mirrors. The photodetectors in the diagram are labelled by the symbols D1-3. Laser 2 is only used for initial alignment	13
2.	The light paths P1 and P2 are drawn in an extended form in Sections 2.1 and 2.2 of this figure respectively. The horizontal and vertical distances on the diagram correspond to the horizontal and vertical distances travelled by the light beam. The width of the optical flats supporting mirrors M0 and M3 is $L/\sqrt{2}$	14
3.	The Bragg cell is illustrated in schematic form in this diagram along with the coordinates used at the Bragg cell (x_0, y_0, o) and the detector (x_1, y_1, z_1)	15

Page

4. This is a schematic diagram of the radio and detector electronics associated with the Mach Zehnder acousto-optic interferometer 16

5. This is a plot of the light intensity, at the detector D3, of the first order diffracted beam resulting from two 75 MHz radio signals applied to the Bragg cells 1 and 2, as a function of the phase difference between the two radio signals measured using a vector voltmeter 17

6. The difference in phase between the radio signals applied to Bragg cells 1 and 2 estimated using the Mach Zehnder acousto-optic interferometer plotted versus the radio phase difference measured using a vector voltmeter. Data are plotted for the frequencies 70, 75, 80 and 90 MHz. The Mach Zehnder acousto-optic interferometer estimate is accurate to ±1.6° over the phase difference range from 30° to 150°. The nonlinear properties of the cosine function cause the error to increase outside this range 18

7. The difference in phase between the radio signals applied to Bragg cells 1 and 2 estimated using the Mach Zehnder acousto-optic interferometer plotted versus the radio phase difference measured using a vector voltmeter. Data are plotted for the frequencies 100, 110 and 120 MHz. The Mach Zehnder acousto-optic interferometer estimate is accurate to ±1.6° over the phase difference range from 30° to 60° for the 100 and 110 MHz data. The 120 MHz data has a larger error ~±3° 19

APPENDIX I RADIO FREQUENCY HEATING EFFECTS ON ACOUSTO-OPTIC PHASE MEASUREMENTS 20

Figure I.1 This is a plot of the light intensity at the detector D3, of the first order diffracted beam resulting from two 75 MHz radio signals applied with no phase difference to the two Bragg cells, plotted versus the elapsed time after radio frequency power was applied to Bragg cell 2 21

Figure I.2 The natural logarithm of the phase difference $\delta = \Delta\phi(t) - \Delta\phi(\infty)$ is plotted versus the elapsed time after radio frequency power has been applied to Bragg cell 2. There are two distinct linear regions of $\ln(\delta)$ versus time 22

1. INTRODUCTION

Acousto-optic (AO) interaction can be used to interface the radio frequency and optical frequency domains of the electromagnetic spectrum(ref.1). With the AO cell at the Bragg angle, both amplitude and phase information is transferred from the radio signal to the first diffraction order of the incident optical beam(ref.2 to 4). By placing two AO cells in an optical interferometer configuration the phase relationship of the first order diffracted beams from these cells can be determined. This optical phase relationship can then be used to determine the relative phase between the two radio signals applied to the AO cells.

2. THE MACH-ZEHNDER ACOUSTO-OPTIC INTERFEROMETER

2.1 Basic optical layout

Most of the essential optics of this device can be described by ray optics, supplemented by optical path length considerations and the principle of superposition. A plan view of the optics of the device is shown in the schematic form in figure 1. The four mirrors M0-3 are arranged in a Mach-Zehnder interferometer configuration(ref.5). This type of interferometer has widely separated paths P1-2 and hence the physical size of any objects such as the Bragg cells 1-2 placed in these paths, does not influence directly the interferometic equations. This can be contrasted with the Young's interferometer where the spacing between the sound beams in the Bragg cells, enters directly into the interferometric equations(ref.4).

Light from laser 1 is split into the two paths P1 and P2 by mirror M0. Radio frequency signals applied to the Bragg cells disperse the laser beam in the direction normal to the page. This dispersed light pattern is detected by detectors D1 and D2. Mirror M3 acts as an optical beam combiner. The two beam components from paths P1 and P2 can be superimposed at the detector D3 by correctly aligning the mirrors M0-M3.

Figure 2 illustrates the vertical progression of the light along paths P1 and P2 in Sections 2.1 and 2.2 respectively. The vertical distance between the undiffracted and the first order diffracted beams at the detector D3 are

$$x_1 = H_1 \sin\theta_1 \tag{1}$$

and

$$x_2 = \left[H_2 + \left(\frac{1}{n} - 1\right) L\right] \sin\theta_2 \tag{2}$$

where H_1 and H_2 are the distances from the cells to the detectors. Mirror M3 has width L and refractice index n.

The beams from paths P1 and P2 can be superimposed at detector D3 by choosing $x_1 = x_2$. If the angle $\theta_1 = \theta_2$ then the choice

$$H_1 = H_2 + \left(\frac{1}{n} - 1\right) L \tag{3}$$

fulfills the requirements $x_1 = x_2$. Under these conditions the same perturbation at each of the Bragg cells 1 and 2 results in the same image at the detector D3.

The phase difference $\Delta\phi$ of the light beams P1 and P2 at the detector D3 is given in terms of their respective optical paths OP1 and OP2 as

$$\Delta\phi = 2\pi(OP1 - OP2)/\lambda \tag{4}$$

where λ is the wavelength of the light. Ignoring the effect of the Bragg cells on the optical paths, these are given as

$$OP1 = G1 + \frac{H1}{\cos\theta_1} + (n-1)L \tag{5}$$

$$OP2 = G2 + \frac{(H2-L)}{\cos\theta_2} + \frac{nL}{\cos\theta_2} \tag{6}$$

where

$$\bar{\theta}_2 = \sin^{-1}\left\{\frac{1}{n}\sin\theta_2\right\} \tag{7}$$

The phase difference calculated from these optical paths is a function of the deflection angle $\theta = \theta_1 = \theta_2$, the width L, and the refractive index of the mirror optical flats. Hence if the effect of the Bragg cells on the optical phase is ignored, the phase difference between the two signals from the paths P1 and P2 is constant for a constant deflection angle. The deflection angle of the Bragg cell is given via the Bragg equation as(ref.6).

$$\theta = 2\sin^{-1}\left\{\frac{\lambda}{2v} f\right\} \tag{8}$$

for an acoustic beam of velocity v and frequency f. The frequency of the acoustic beam is derived from the radio signal which is applied to the transducer of the Bragg cell. See figure 3. Thus the optical devices which are external to the Bragg cell introduce a phase difference $\Delta\phi_{inst}(f)$ which depends only on the frequency of the radio signal applied to the Bragg cells.

2.2 Fourier optics and the transmission function for Bragg diffraction

In this section Fourier optics will be used to explain the influence of the Bragg cell on the phase of the first order diffracted beam(ref.7). Let the monochromatic light wave incident on the Bragg cell as shown in figure 3, be expressed by the electric field

$$\underline{E}(x,y,z,t) = (E_x(x,y,z,t),\ 0,\ 0) \tag{9}$$

where

$$E_x(x,y,z,t) = R_e[E(x_o,y_o)\exp(-i\{2\pi\nu t - kz - \phi_i\})] \quad (10)$$

ν is the optical frequency with wave number k,

ϕ_i is the initial phase of the wave at t=z=0, and

$E(x_o,y_o)$ is the normalised amplitude distribution of the optical wave.

The electric field of the upper first diffraction order is given at the point

$$\underline{r}_1 = (x_1,y_1,z_1)$$

in the region to the right of the Bragg cell by the Fresnel approximation as (ref.7).

$$E_x^{\Delta t}(\underline{r}_1, t) = \alpha(\underline{r}_1)\, F_{z_1}\{T(\underline{\rho}_o, t - \Delta t)\, E_x(\underline{\rho}_o, z_o, t)\, \beta(\underline{\rho}_o, z_1)\} \quad (11)$$

where

$$\underline{\rho}_o = (x_o,y_o) \; ; \; \underline{\rho}_1 = (x_1,y_1) \quad (12)$$

$$\alpha(\underline{r}_1) = -i2\pi k z_1 \exp(ikz_1) \exp\left(\frac{ik\rho_1^2}{2z_1}\right) \quad (13)$$

$$\beta(\underline{\rho}_o, z_1) = \exp\left(\frac{ik\rho_1^2}{2z_1}\right) \quad (14)$$

and

$$F_{z_1}\{g(\underline{\rho}_o)\} = \int_{-\infty}^{\infty} g(\underline{\rho}_o)\exp\left(\frac{-k\underline{\rho}_o\cdot\underline{\rho}_1}{z_1}\right) d^2\rho_o \quad (15)$$

The function $T(\underline{\rho}_o,t-\Delta t)$ is a complex transmission function for the Bragg cell.

The input to the piezoelectric transducer of the Bragg cell (see figure 3) is an electromagnetic signal of the form

$$V(t-\Delta t) = A(t-\Delta t)\cos(2\pi f(t-\Delta t)) \quad (16)$$

where Δt is an arbitrary time delay.

If the time derivative $\frac{dA}{dt}$ of the modulation term A is much less than the

reciprocal $\frac{1}{\Delta t}$ of the time delay Δt, then the time delay can be ignored in the modulation term. Thus an approximate form of the input signal is

$$V(t - \Delta t) = A(t) \cos(2\pi f(t-\Delta t)) \tag{17}$$

The piezolectric transducer launches an acoustic wave across the Bragg cell which is given within a constant as(ref.4).

$$S(x_o - v(t - \Delta t)) = A(x_o - vt) \exp\left(-\gamma(f)\left(x_o + \frac{D}{2}\right)\right)\cos\left(2\pi f\left(\frac{x_o}{v} - (t - \Delta t)\right)\right) \tag{18}$$

The acoustic wave is attenuated as it propagates across the aperture which is of length D in the x direction, γ is the acoustic loss coefficient in Np/m and is a function of frequency.

In the Bragg diffraction regime of acousto-optics one of the first diffraction orders can be made to dominate the diffracted energy.

If the upper first diffraction order is chosen to be dominant, then the optical transmission function which projects out only this diffraction order from the incident light beam is(ref.4).

$$T(x_o,y_o,t - \Delta) = \text{rect}\left(\frac{x_o}{D}\right) \text{rect}\left(\frac{y_o}{y}\right) i\psi_B(x_o - vt) \exp\left(-\gamma(f)\left(x_o + \frac{D}{2}\right)\right) \exp\left(i2\pi f\left(\frac{x_o}{v} - (t - \Delta t) + \phi_o\right)\right) \tag{19}$$

where

$$\psi_B(x_o - vt) = K_B A(x_o - vt), \psi_{Bmax} << 1 \tag{20}$$

K_B is a constant for a given Bragg cell.

Y is the length of acoustic beam in the y direction and the acoustic profile is assumed to be uniform in this direction.

ϕ_o is the phase of the modulation at x = 0 and $(t-\Delta t) = 0$.

Equation (19) can be factorised in the form

$$T(x_o,y_o,t-\Delta t) = T(x_o,y_o,t)\exp(i2\pi f\Delta t) \tag{21}$$

Hence in this approximation, the time delay changes the phase of the transmission function by

$$\phi_{\Delta t} = 2\pi f\Delta t \tag{22}$$

By substituting equation (21) in equation (11) the electric field at the point $\underline{r}_1$ is found to include a phase component resulting from the applied radio signal $\phi_{\Delta t}$ that is

$$E_x^{\Delta t}(\underline{r}_1, t) = E_x^{o}(\underline{r}_1, t) \exp(i\phi_{\Delta t}) \tag{23}$$

2.3 The Fourier transform configuration

If an aberration free lens is placed between a Bragg cell and the detection point r_1, such that the Bragg cell and the detection point lie on conjugate focal planes of the lens, then equation (11) takes the special form(ref.4,7)

$$E_x^{\Delta t}(\underline{\rho}_1, z_1, t) = K_1 \int_{-\infty}^{\infty} E_x^{o}(\underline{\rho}_o, z_o, t) \, T(\underline{\rho}_o, t) \exp\left(-i\left(\frac{k}{F}\right)\underline{\rho}_o \, \underline{\rho}_1\right) d^2\rho_o \exp(i\phi_{\Delta t}) \tag{24}$$

where a constant phase factor has been dropped, $K_1 = \frac{1}{i2F}$ and F is the focal length of the lens. Thus the electric field in the detector plane is a scaled Fourier transform of the function

$$h(\underline{\rho}_o, t) = E_x^{o}(\rho_o, z_o, t) T(\underline{\rho}_o, t - \Delta t) \tag{25}$$

This function can be rewritten as

$$h(\underline{\rho}_o, t) = y_{\Delta t}(x_o - vt) \, \omega(\underline{\rho}_o) \tag{26}$$

where

$$y_{\Delta t}(x_o - vt) = A(x_o - vt) \exp i\left(\frac{2\pi f}{v}(x_o - v(t - \Delta t))\right) \tag{27}$$

$$\omega(\underline{\rho}_o) = E_o(\underline{\rho}_o) \operatorname{rect}\left(\frac{x_o}{D}\right) \operatorname{rect}\left(\frac{y_o}{Y}\right) \exp\left[-\gamma(f)\left(x_o + \frac{D}{2}\right)\right] \tag{28}$$

Thus the diffracted instantaneous amplitude distribution in the detector focal plane is the one sided Fourier transform of the weighted input signal $h(\underline{\rho}_o, t)$. Compare equations (17) and (27).

2.4 Determination of optical phase differences from intensities

The detectors D1 and D3 can be arranged so that the distance the undiffracted beam travels from Bragg cell 1 to each of these detectors is the same. Also two sets of coordinates $\underline{r}_1$ and $\underline{r}_3$ can be chosen which have their origins at the point of intersection between the undiffracted beam

and detectors D1 and D3 respectively. Further, the Z axes can be aligned with the undiffracted beam and the X axes aligned horizontally for each of these coordinates.

If the path P2 is obstructed then the light intensity pattern I_3^1 at detector D3 is a scaled version of the light intensity I_1 at detector D1. Thus using the above coordinates

$$I_3^1 (\underline{r}_3,t) = R_1 I_1 (\underline{r}_1 , t) \tag{29}$$

where $r_3 = r_1$ is implied by this equation. A similar argument for Bragg cell 2 and detector D2 leads to

$$I_3^2 (\underline{r}_3,t) = R_2 I_2 (\underline{r}_2,t) \tag{30}$$

If the signals applied to the Bragg cells are the same except that one is delayed by an amount Δt then the superposition law for light gives

$$I_3 = I_3^1 + I_3^2 + 2\sqrt{I_3^1 I_3^2} \cos(\Delta\phi) \tag{31}$$

where the coordinates $(\underline{r}_3,t)$ have been suppressed and the difference in optical phase of the two light beams at detector D3 is $\Delta\phi$. The ratios R1 and R2 can be measured by obstructing the appropriate path as mentioned before. With these two ratios and the measured intensities, I_1, I_2 and I_3 then the optical phase difference $\Delta\phi$ can be determined using equations (29), (30) and (31).

2.5 Simultaneous radio phase and frequency measurements

If the signals entering the two Bragg cells consists of different frequencies which are present simultaneously at each of the Bragg cells, but which differ in phase, then the frequency spectrum of these signals can be displayed at either detector D1 or D2 by introducing a fourier transform lens as previously described. A similar lens placed in front of the detector D3 also produces a frequency spectrum however the intensity distribution of this spectrum is given by the superposition formula of equation (31).

Hence for each frequency component f of the input signals a comparison of the peak intensity from detector D1 and detector D3 using equation (31) yields the phase difference $\Delta\phi(t)$ between the diffracted beams for that frequency at detector D3.

$$\Delta\phi(f) = \cos^{-1}\left[\frac{I_3}{2R_1 I_1} - 1\right] \tag{32}$$

since $R_1 = R_2$ and $I_1 = I_2$ for the interferometer previously described. By subtracting from this phase difference the instrument phase difference $\Delta\phi_{inst}(f)$ the radio phase difference $\Delta\phi_{\Delta\tau}(f)$ can be determined at that frequency

$$\Delta\phi_{\Delta t}(f) = \Delta\phi(f) - \Delta\phi_{inst}(f) \quad (33)$$

The instrument phase difference can be measured in practice by using radio signals with known phase difference. This device therefore provides simultaneously the frequency spectrum of two compound radio signals and the phase relationship between corresponding frequency components of these signals.

2.6 Comparison with the Young's interferometer configuration

A number of papers have already been published which consider the use of a Young's interferometer configuration to produce acousto-optic signal processors which simultaneously measure frequency and phase differences(ref.2 to 4). The Mach-Zehnder interferometer offers some advantages in respect to the Young's interferometer in producing this type of signal processor. The sizes of the Bragg cells do not enter directly into the interferometric equations in the Mach-Zehnder configuration. This enables the use of existing bulk Bragg cell technology to be used to obtain systems with high diffraction efficiency and accurate phase difference measurement capability. Further the Mach-Zehnder interferometer configuration only needs three (two) linear photodetector arrays rather than the two dimensional photodetector required for the Young's interferometer. The linear photodetectors are faster and cheaper than the two dimensional photodetectors. Finally the postprocessing needed for the Mach-Zehnder configuration is simpler than that for the Young's configuration. Its main disadvantage is that it includes four accurately aligned mirrors which are not necessary in the Young's interferometer.

3. EXPERIMENTAL STUDIES OF THE MACH-ZEHNDER ACOUSTO-OPTIC INTERFEROMETER

A Mach-Zehnder acousto-optic interferometer of the type previously described has been constructed, details of its construction, and measurements made using it are described in the following sections.

3.1 The optical system

The optics were assembled on a Newport Research Corporation (NRC) pneumatically isolated eight foot by six foot optical table. The laser was a model L23DA power technology helium neon laser (λ = 0.6328 μm). This laser was arranged so that the electric polarisation vector, of the emitted light, was in the horizontal plane. The light beam emitted from the laser was Gaussian in profile and had a full width half maximum of 0.8 mm. This beam was then expanded 43 times by using a model 900 NRC beam expanding collimator. A 10 μm diameter pinhole was used at the focal point of the entrance lens as a spatial filter.

The mirrors were fabricated by using a suitable thickness aluminium film on a ½ inch thick, 2 inch square optical flat. These mirrors had reflection transmission ratios of 1:1 for mirrors M0 and M3 and 9:1 for mirrors M1 and M3.

The detectors D1 and D2 were Hewlett Packard (HP) 5082-4220 PIN photodiodes with a 0.4 mm diameter stop placed in front of the active area. The detector D3 was fabricated using the same type of photodiode mounted in a light tight box with a 25 μm pinhole. The photodiode was placed close enough to the pinhole that the diffraction pattern from the pinhole was contained by the active area of the photodiode. All of these photodiodes were connected to μA740 operational amplifiers operating as current amplifiers with a gain of a million. The outputs of these amplifiers were

then multiplexed into a HP3478A digital multimeter which was connected via a IEEE-488 data bus to a HP-87 computer. See figure 4.

3.2 Alignment of the interferometer

The mirrors M1 and M2 were brought into parallel alignment by the following procedure. The laser was placed in the position indicated by laser 2 in figure 1 Mirrors M1 and M2 are 90% reflecting and in this configuration formed a Fabry Perot interferometer cavity. The laser beam was set perpendicular to mirror M2 by observing the position of the reflected beam on the face of the laser. Mirror M0 was then adjusted so that the multipath images in the cavity were superimposed. Fabry Perot fringes appeared as the images became superimposed and these were formed into a concentric pattern. Further alignment of the mirrors wasachieved by using the beam expander. The large Fabry Perot fringes obtained with the expanded light beam allowed more critical centering of the image and hence more accurate alignment of the mirrors M1 and M2. The laser was then returned to its usual position marked as laser 1 in figure 2. However the beam expander was not used in the initial alignment of mirrors M0 and M3. These mirrors were set roughly parallel to mirrors M1 and M2. Mirror M0 was then adjusted so that the two beams from path P1 and P2 were superimposed on the reflecting surface of mirror M3. The reflected and transmitted beams were observed on a screen at a distance of a few centimetres from the mirror in the direction of detector D3 (see figure 1). The mirror M3 was then adjusted until the beams were superimposed on the screen. The mirrors were mounted on three point mounts. With these mounts it was found that mirror M0 then needed to be readjusted to superimpose the beams on the surface of mirror M3. Two or three interactions of this alignment procedure resulted in the observation of interference fringes on the surface of the mirror and at the screen. When the beam expanding telescope was placed in position in front of the laser, fringes could be obtained which had a periodicity greater than twice the length of the 5 cm size of the mirrors. This complete alignment procedure took only a few minutes.

It was found that the movement of air across the optical bench caused the Mach-Zehnder fringes to fluctuate on a time scale of a few seconds. In order to increase the stability of these fringes a perspex box was placed over the interferometer. With the perspex box in place, the fringes were stable for typically tens of minutes. At each frequency the full phase measurements were completed in less than thirty seconds with the aid of computer control and sampling. Hence the fringes were stable over the period of measurement.

3.3 Wave front distortion of the Bragg cells

The inclusion of either of the Bragg cells (Isomet 1025C-1 modulators) in the aligned interferometer, as indicated in figure 1, resulted in the observation of fringes across the Bragg cell image at detector D3. This fringe pattern had a spacing between maxima of typically 3 mm and resulted from wave front distortion of the light, caused by the Bragg cell. By adjusting the interferometer to create a narrowly spaced Mach Zehnder fringe pattern and then placing the Bragg cell in the interferometer the maximum wave front distortion could be measured from the displacement of the Mach-Zehnder fringes; this was found to be $1\frac{1}{2}\lambda$. This wave front distortion prohibited the use of large regions of the Bragg cells for phase measurements

such as have previously been described. However by using a small detector 25 μm diameter) excellent verification of equation (23) was obtained and hence of the general theory that led to this equation. Bragg cells with better wave front distortion (λ/10) should enable accurate phase difference and accurate power spectrum information to be obtained simultaneously.

3.4 Radio frequency electronics

Figure 4 includes a schematic of the radio frequency (RF) system used to make the measurements presented in this paper. The radio signal source was a Rockland 5600 frequency synthesiser. The output from this was split using a divider and passed through 30 dB attenuators into each channel. These attenuators performed two functions. Firstly they reduced the output of the synthesiser to one microwatt per channel. This power level was required by the PIN diode switched delay lines. The attenuators also provide isolation between the two channels. The RF signals were passed from the attenuators to the computer controlled delay lines. These delay lines were fabricated using striplines that were PIN diode switched, offering the possibility of 256 possible delays. The output from these delay lines was amplified by HP8447D preamplifiers. A variable attenuator was placed after the preamplifier in channel one to compensate for any gain mismatches between the two channels. The power amplifiers were constructed using Motorola MHW591 hybrid integrated circuits. The RF power levels from each of the channels were measured using a HP435A power meter. The phase difference beween the two channels was measured using a HP8405A vector voltmeter.

3.5 Measurements of the Radio Phase Difference

Figure 5 is a plot of the light intensity at the detector D3 of the first order diffracted light beam resulting from half watt, 75 MHz radio signals applied simultaneously to the two Bragg cells 1 and 2, as a function of the phase difference between the two radio signals as measured by the vector-voltmeter. The cosine form of this intensity as predicted by equation (31) is apparent with an instrumental phase offset $\Delta\phi_{inst} = 50^{\circ}$. Similar results to this were obtained at 70, 80, 90, 100, 110, and 120 MHz.

The values of the ratios R_1 and R_2 in equations (31) and (32) were determined in two ways at each frequency. Firstly by switching off the radio signal to one of the Bragg cells 2 or 1 then the light intensity at detector D3 was $I_3 = R_1.I_1$ or $I_3 = R_2.I_2$ respectively, where I_1 and I_2 are the intensities at detectors D1 and D3 respectively. thus the ratio were evaluated as $R_1 = I_1/I_3$ and $R_2 = I_2/I_3$. The second approach to determining R_1 and R_2 was to monitor the three intensities I_1, I_2 and I_3 as the radio phase difference was changed and fit the intensity data using equation (31) with R_1, R_2 and $\Delta\phi_{\Delta t}$ as free parameters. Both these methods gave similar value for R1 and R2. Using the values of R_1 and R_2, obtained for each frequency, equation (31) was inverted and the optical phase difference obtained as

$$\Delta\phi = \cos^{-1}(h) \qquad (34)$$

$$h = \frac{I_3 - R_1.I_1 - R_2.I_2}{2\sqrt{R_1.R_2.I_1.I_2}} \tag{35}$$

The instrumental phase difference $\Delta\phi_{inst}$ was taken to be the optical phase difference when the radio phase was zero. An estimate of the radio phase difference $\Delta\phi_0$ was obtained by subtracting the instrumental phase difference from the optical phase difference ie

$$\Delta\phi_o = \Delta\phi - \Delta\phi_{inst} \tag{36}$$

Figures 6 and 7 are plots of the estimated phase difference $\Delta\phi_o$ versus the radio phase difference measured with the vector voltmeter for the frequencies, 70, 75, 80, 90, 100, 110 and 120 MHz. These figures show that the estimated phase difference is a good estimate of the radio phase difference over the range 30 to 150°. The error bars $\sigma(\Delta\phi_o)$ on these figures are standard deviations obtained by using a value of 2% for the error $\sigma(I)$ in the measurement of the optical intensities and using small error analysis applied to equations (34) and (35)(ref.8).

The value of 2% for the standard deviation of the intensities was obtained by performing repeated measurements of these quantities, typically a hundred samples. The error $\sigma(\Delta\phi_o)$ is given from small error analysis as(ref.8).

$$\sigma(\Delta\phi_o) = \frac{1}{\sqrt{1 - h^2}} \left\{ \sum_{i=1}^{3} \left(\frac{\partial h}{\partial I_i} \right)^2 \sigma^2(I_i) + \sum_{i=1}^{2} \left(\frac{\partial h}{\partial R_j} \right)^2 \sigma^2(R_j) \right\}^{\frac{1}{2}} \tag{37}$$

The dependence of this equation on the radio phase difference $\Delta\phi_R$ is dominated by the common factor

$$K = \frac{1}{\sqrt{1 - h^2}} \tag{38}$$

The function h covers the range [-1,1] as the phase difference $\Delta\phi$ covers the domain [0,180].

One further source of error was studied and that was the effects of the RF power level on the instrumental phase difference $\Delta\phi_{inst}$. This error was found to be significant and is discussed in an appendix.

4. CONCLUSIONS

The difference in phase between two radio signals can be measured by applying them to two Bragg cells situated in opposite arms of a Mach-Zehnder interferometer, and observing the intensity of the light from each of the Bragg cells and the output of the interferometer. Measurements in this paper

verify that a phase change is introduced into the first order diffracted beam resulting from Bragg accoustooptic diffraction, which corresponds to a phase change of the radio signal applied to the Bragg cell. Hence it is indicated that by using Bragg cells with low wave front distortion (~λ/10) the Mach-Zehnder acousto-optic interferometer configuration described in this paper can be used to obtain simultaneously the frequency spectrum of two radio signals and the relative phase of the two signals as a function of frequency.

The Mach-Zehnder acousto-optic interferometer (MZAOI) has some advantages over Young's acousto-optic interferometer configurations (YAOI). There is no trade off between diffraction efficiency and direction of arrival accuracy for the MZAOI. Commercially available Bragg cells can be used in the MZAOI. The MZAOI uses linear photodetector arrays which are faster and cheaper than the two dimensional photodetector arrays required for the YAOI. The phase difference post processing is simpler for the MZAOI than it is for the YAOI.

5. ACKNOWLEDGEMENTS

I would like to acknowledge the technical assistance of Mr Chris Cocks in relation to the experimental section of this paper.

REFERENCES

No.	Author	Title
1	Korpel, A.	"Acousto-optics in Applied Optics and Optical Engineering VI". Kingslake, R. and Thompson, B.J., Eds (New York Academic Press, 1980), Chapter 4, pp 89 - 136
2	Lambert, L.B., Arm, M. and Aimette, A.	"Electro-optical Signal Processors for Phased Array Antennas in Optical and Electro-optical Information Processing". Tippet et al, J.T., Eds (M.I.T. Press, Cambridge, 1965), Chapter 38, pp 715-748
3	Coppock, R.A. and Croce, R.F.	"Wideband Optical Channelizer for Simultaneous Frequency and Direction Finding, in Proceedings Acousto-Optic Bulk Wave Devices". (SPIE, Monterey, 1979), pp 124-129
4	Lee, J.P.Y.	"Appl Opt 22, 867-72 (1983)".
5	Born, M. and Wolf, E.	"Principles of Optics". (Pergamon Press 1980)
6	Korpel, A.	"Proc IEEE 69, 48-53 (1981)".
7	Goodman, J.W.	"Introduction to Fourier Optics". (McGraw-Hill 1968)
8	Baird, D.C.	"Experimentation: An Introduction to Measurement Theory and Experiment Design". (Prentice-Hall Inc 1962)

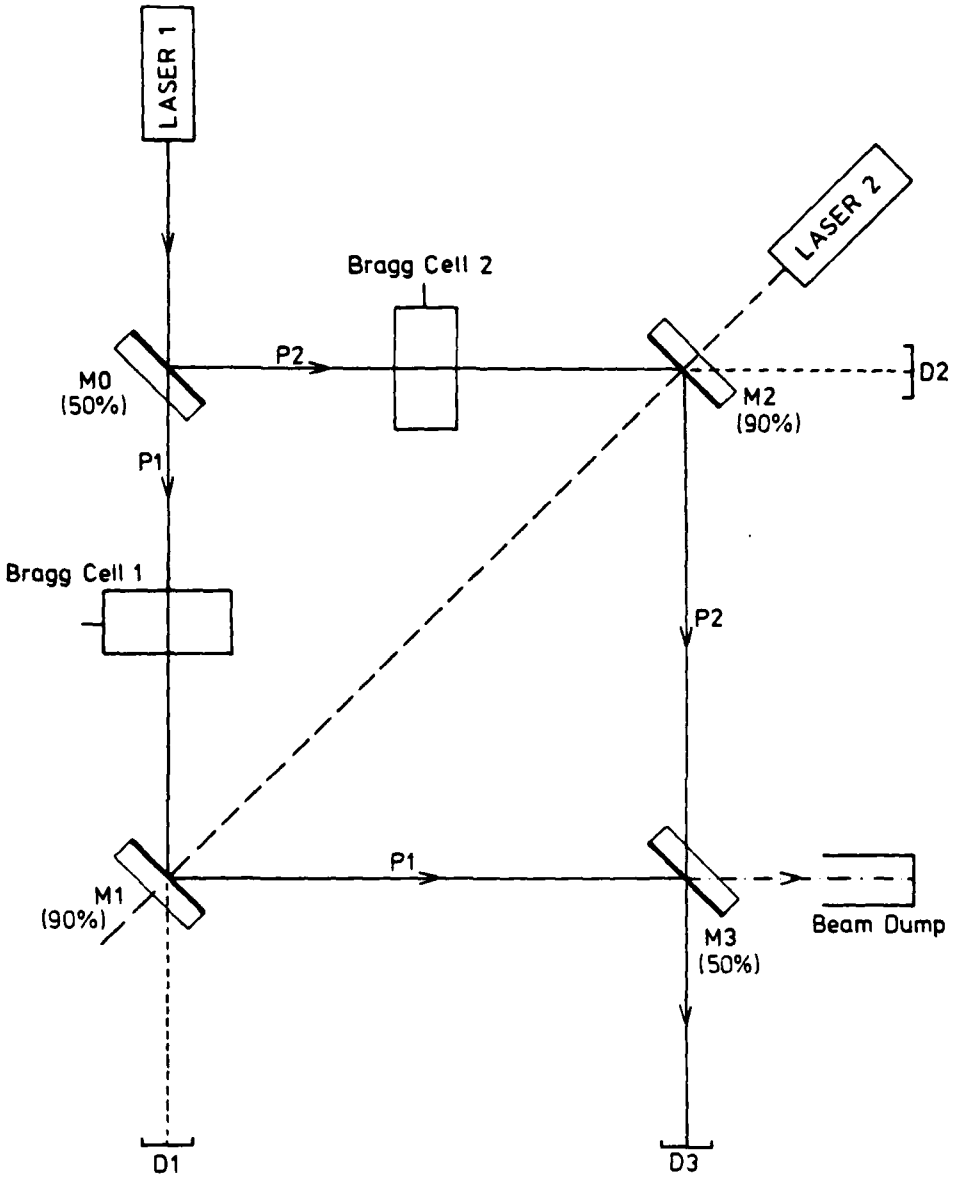

Figure 1. This is a Schematic diagram of the optics of the Mach Zehnder acousto-optic interferometer. The labels M0 and M3 denote 50% reflecting mirrors, and M1 and M2 denote 90% reflecting mirrors. The photodetectors in the diagram are labelled by the symbols D1-3. Laser 2 is only used for initial alignment

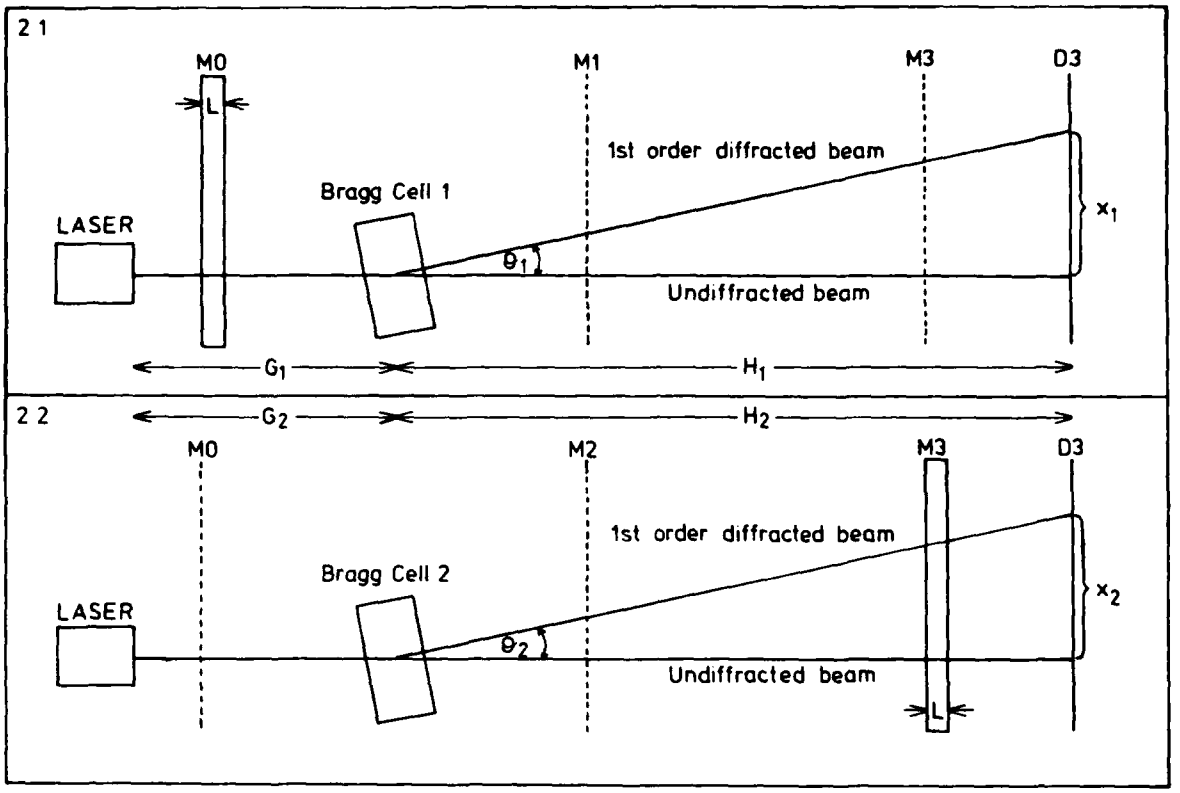

Figure 2. The light paths P1 and P2 are drawn in an extended form in Sections 2.1 and 2.2 of this figure respectively. The horizontal and vertical distances on the diagram correspond to the horizontal and vertical distances travelled by the light beam. The width of the optical flats supporting mirrors M0 and M3 is $L/\sqrt{2}$

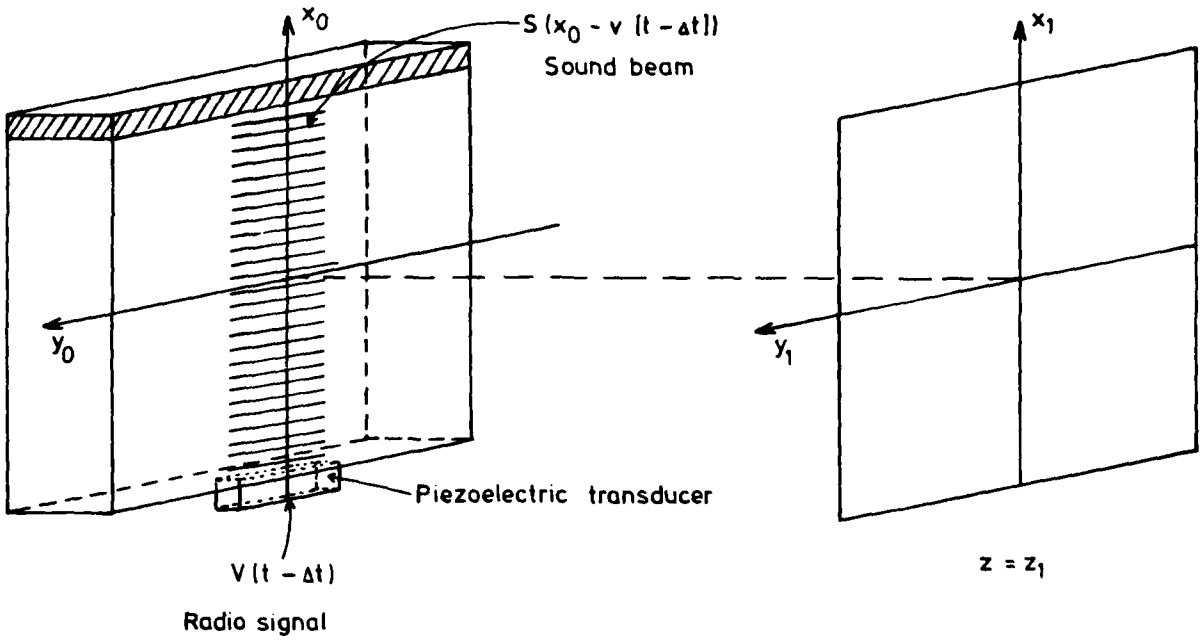

Figure 3. The Bragg cell is illustrated in schematic form in this diagram along with the coordinates used at the Bragg cell (x_0, y_0, o) and the detector (x_1, y_1, z_1)

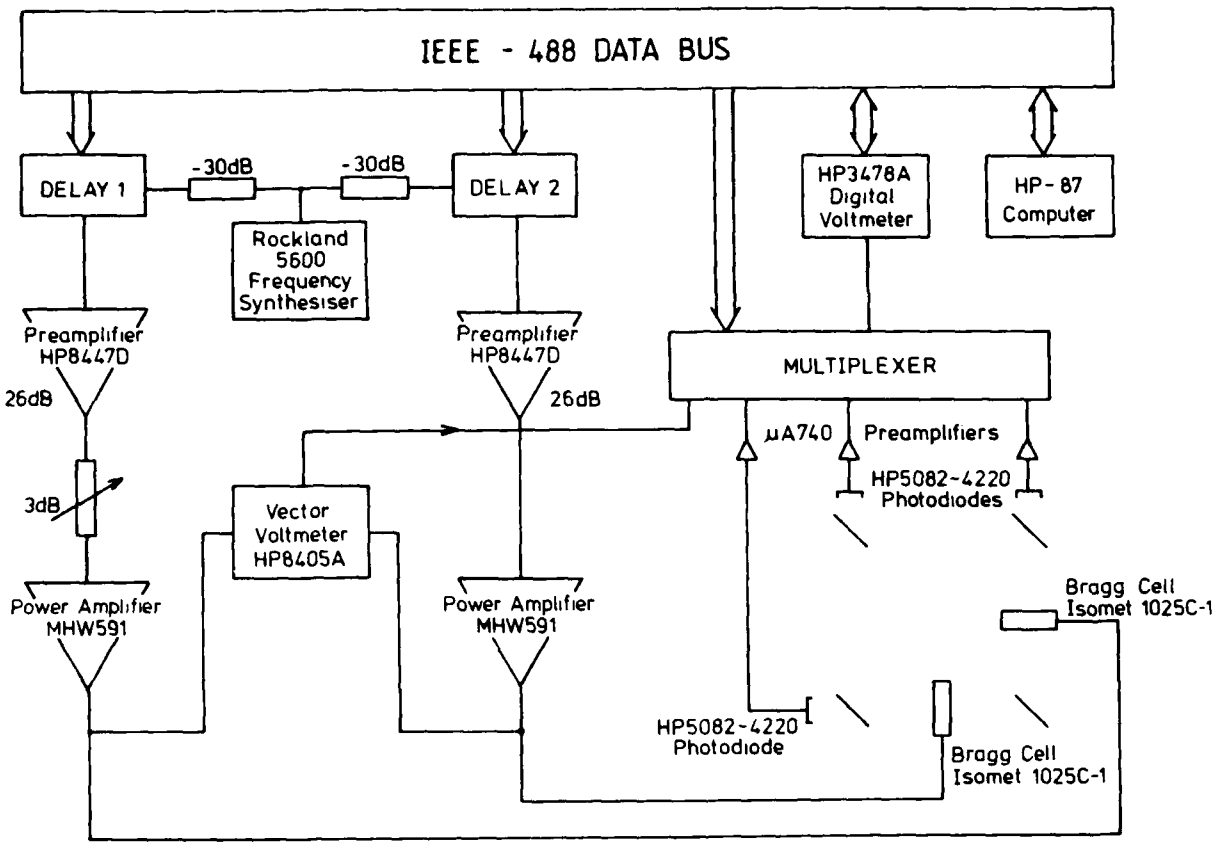

Figure 4. This is a schematic diagram of the radio and detector electronics associated with the Mach Zehnder acousto-optic interferometer

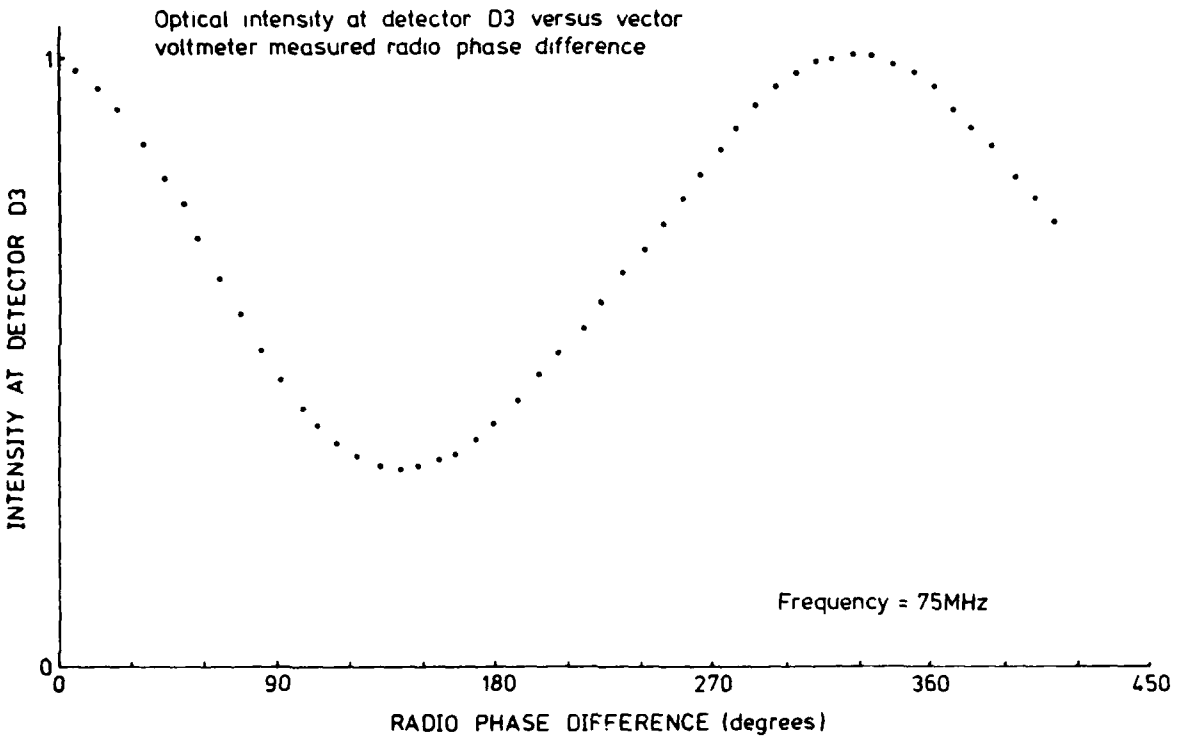

Figure 5. This is a plot of the light intensity, at the detector D3, of the first order diffracted beam resulting from two 75 MHz radio signals applied to the Bragg cells 1 and 2, as a function of the phase difference between the two radio signals measured using a vector voltmeter

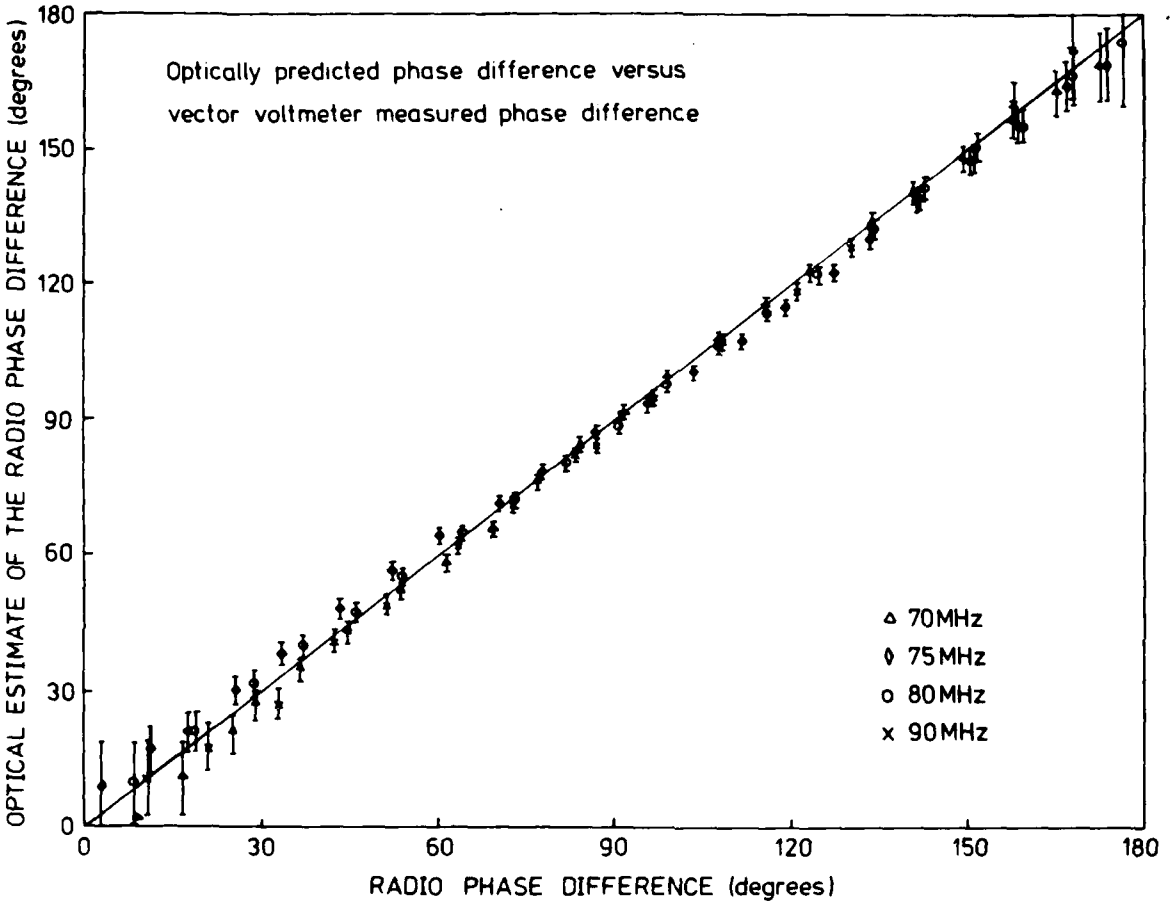

Figure 6. The difference in phase between the radio signals applied to Bragg cells 1 and 2 estimated using the Mach Zehnder acousto-optic interferometer plotted versus the radio phase difference measured using a vector voltmeter. Data are plotted for the frequencies 70, 75, 80 and 90 MHz. The Mach Zehnder acousto-optic interferometer estimate is accurate to $\pm 1.6^{o}$ over the phase difference range from 30^{o} to 150^{o}. The nonlinear properties of the cosine function cause the error to increase outside this range

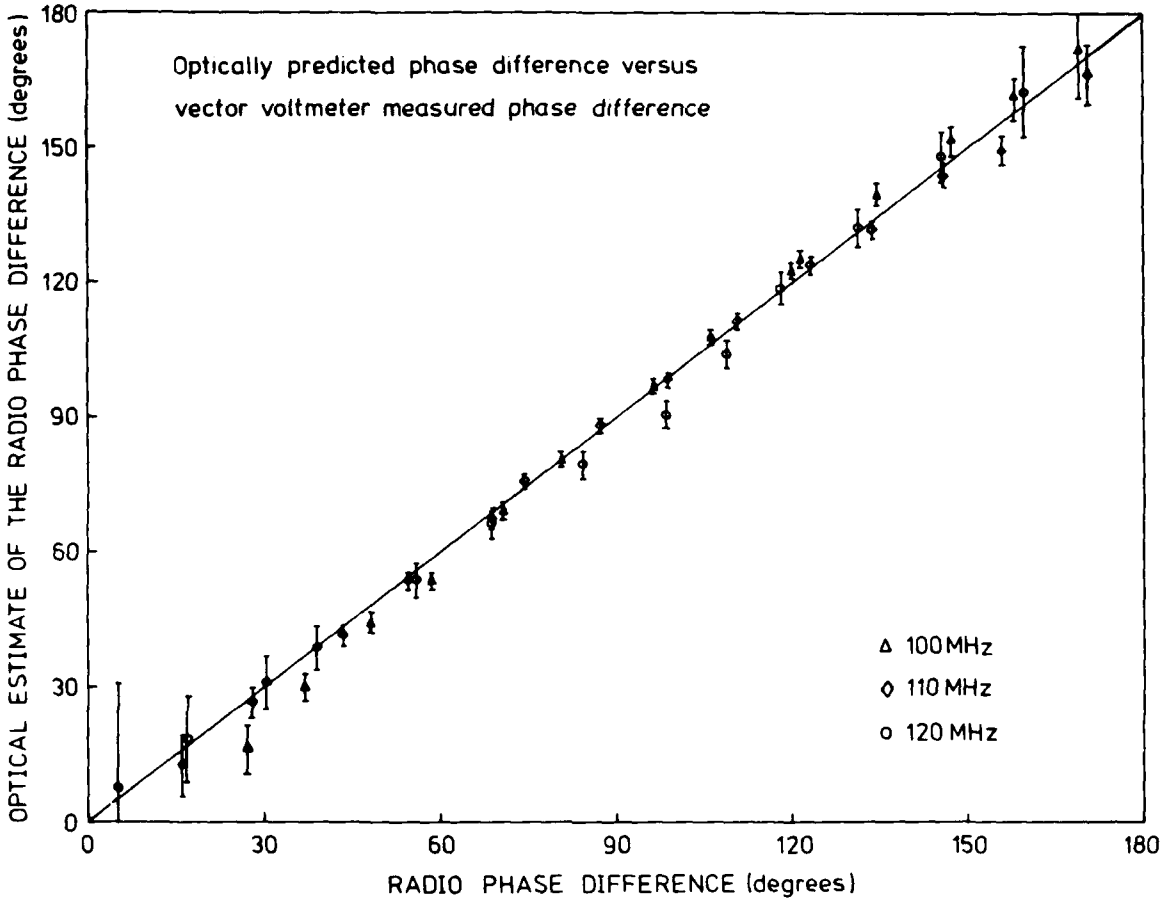

Figure 7. The difference in phase between the radio signals applied to Bragg cells 1 and 2 estimated using the Mach Zehnder acousto-optic interferometer plotted versus the radio phase difference measured using a vector voltmeter. Data are plotted for the frequencies 100, 110 and 120 MHz. The Mach Zehnder acousto-optic interferometer estimate is accurate to $\pm 1.6^{\circ}$ over the phase difference range from 30° to 60° for the 100 and 110 MHz data. The 120 MHz data has a larger error $\sim \pm 3^{\circ}$

APPENDIX I

RADIO FREQUENCY HEATING EFFECTS ON ACOUSTO-OPTIC PHASE MEASUREMENTS

Measurements were made which showed that the optical phase of the first diffraction order was strongly dependent on the power of the radio frequency (RF) signal applied to the Bragg cell. A half watt RF signal of 75 MHz frequency was applied to the Bragg cell 1 in the Mach-Zehnder interferometer see figure 1. This signal was maintained to that cell for a time period of one hour. After this time it was considered that this cell had reached thermodynamic equilibrium. During this time Bragg cell 2 had no radio signal applied to it. A half Watt signal for 75 MHz frequency was applied to cell 2 after the hour had elapsed. The phase difference between the two radio signals applied to the two Bragg cells 1 and 2 was held constant. The intensity observed at the detector D3 in figure 1 is plotted, as a function of the elapsed time after Bragg cell 2 was turned on, in figure I.1. This figure shows that heating of the Bragg cell due to the applied radio signal, significantly affects the phase of the first order diffracted beam for the first few minutes after the signal has been applied to the cell.

By applying the principle of superposition the intensity at the optical detector D3 can be used to predict the optical phase difference $\Delta\phi$ as a function of time.

$$\Delta\phi(t) = \cos^{-1}\left\{\frac{I_3(t) - I_1 - I_2}{2\sqrt{I_1 I_2}}\right\} \qquad (I.1)$$

where I_1 and I_2 are the intensities of the light from Bragg cell 1 and 2 respectively at detector D3. The intensity $I_3(t)$ is the intensity at D3 as a result of the superposition of the light from each of the Bragg cells.

The phase difference $\Delta\phi(t)$ could be considered to be directly proportional to the integrated temperatures in the Bragg cell along the light ray which terminates at the detector D3. If further it is assumed that the temperature approaches equilibrium in an exponential manner then

$$\Delta\phi(t) = A \exp\left(-\frac{T}{\tau}\right) + \Delta\phi(\infty) \qquad (I.2)$$

where t is the time constant with which the thermodynamic system approaches equilibrium and $\Delta\phi(\infty)$ is the phase difference at equilibrium. In figure I.2 the natural logarithm of $\Delta\phi(t)-\Delta\phi(\infty)$ is plotted versus time elapsed from the commencement of RF to power to the Bragg cell BC2.

This figure indicates that there are two regions in which the simple mathematical model described above approaches reality and these two regions are characterised by different time constants. It is possible that the first region 0 to 1 min corresponds to the local heating of the transducer cavity and coupling layers. This heating would affect the phase of the acoustic beam relative to the applied electrical signal. The later region could result from the optical effects of crystal heating referred to before. Though this RF heating effect is important it can be relatively simply compensated for by ensuring that the total RF power applied to each of the Bragg cells is constant. This could be achieved by supplying an auxilary radio signal at one frequency and adjusting the level of this auxiliary signal to maintain a constant total RF power to the cells.

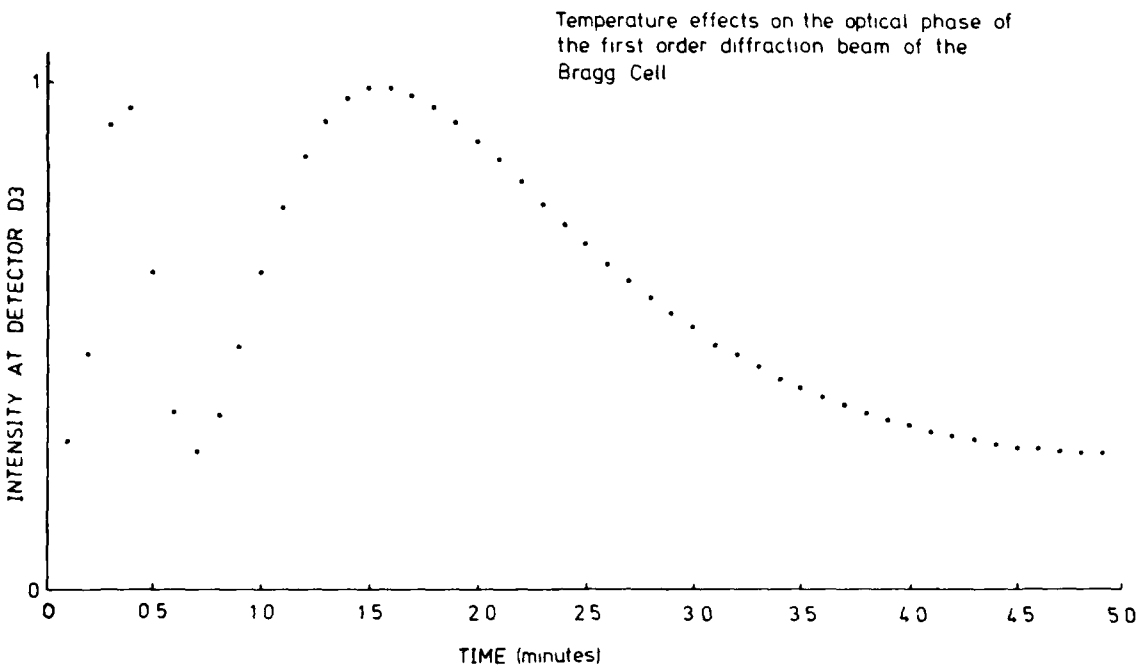

Figure I.1 This is a plot of the light intensity at the detector D3, of the first order diffracted beam resulting from two 75 MHz radio signals applied with no phase difference to the two Bragg cells, plotted versus the elapsed time after radio frequency power was applied to Bragg cell 2

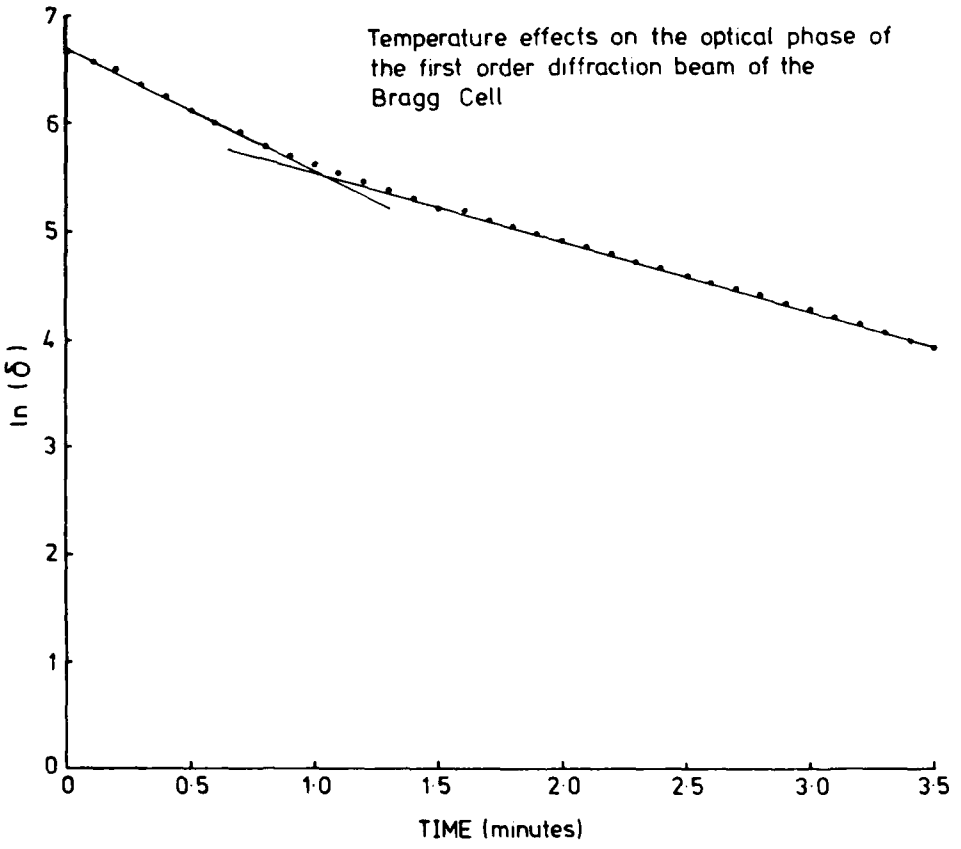

Figure I.2 The natural logarithm of the phase difference $\delta = \Delta\phi(t) - \Delta\phi(\infty)$ is plotted versus the elapsed time after radio frequency power has been applied to Bragg cell 2. There are two distinct linear regions of $\ln(\delta)$ versus time

DISTRIBUTION

	Copy No.
EXTERNAL	
United Kingdom	
Defence Science Representative, London	Cnt Sht Only
Institution of Electrical Engineers	1
British Library, Lending Division, Boston Spa, Yorks	2
In United States of America	
Counsellor, Defence Science, Washington	Cnt Sht Only
Engineering Societies Library	3
In Australia	
Department of Defence	
Chief Defence Scientist	4
Deputy Defence Scientist	
Controller, External Relations, Projects and Analytical Studies	
Superintendent, Science Programs and Administration	
Director, Joint Intelligence Organisation	5
Defence Exchange Centre Defence Information Services Branch for:	
Microfilming	6
United Kingdom, Defence Research Information Centre (DRIC)	7 - 8
United States, Defense Technical Information Center	9 - 20
Canada, Director, Scientific Information Services	21
New Zealand, Ministry of Defence	22
National Library of Australia	23
Director General, Army Development (NSO), Russell Offices for ABCA Standardisation Officers	
UK ABCA representative, Canberra	24
US ABCA representative, Canberra	25
Canada ABCA representative, Canberra	26
NZ ABCA representative, Canberra	27

Defence Library, Campbell Park	28
Library, Aeronautical Research Laboratories	29
Library, Materials Research Laboratories	30
Library, H Block, Victoria Barracks, Melbourne	31
Library, RAN Research Laboratory	32
Department of Defence Support	
Deputy Secretary (Manufacturing)	33
Deputy Secretary (Materiel and Resources)	
Controller, Defence Aerospace Division	
Controller, Munitions Division	
Library, DDS Central Office	34
Director, Industry Development, SA/NT	Cnt Sht Only
WITHIN DRCS	
Director, Electronics Research Laboratory	35
Superintendent, Optoelectronics Division	36
Superintendent, Electronic Warfare Division	37
Senior Principal Research Scientist, Electronic Warfare Division	38
Principal Officer, Information and Signal Processing Group	39
Principal Officer, Electronic Warfare Techniques Group	40
Principal Officer, Communications Electronic Warfare Group	41
Principal Officer, Infrared and Optical Countermeasures Group	42
Principal Officer, Optical Techniques Group	43
Principal Officer, Optoelectronic Device Physics Group	44
Dr R.M. Hawkes, Information and Signal Processing Group	45
Mr D.A.B. Fogg, Information and Signal Processing Group	46
Dr S.T. Hood, Information and Signal Processing Group	47
Mr A.D. Doolette, Information and Signal Processing Group	48
Author	49 - 50
DRCS Library	51 - 52
Spares	53 - 58

DOCUMENT CONTROL DATA SHEET

Security classification of this page: UNCLASSIFIED

1 DOCUMENT NUMBERS	
AR Number:	AR-004-113
Series Number:	ERL-0319-TR
Other Numbers:	

2 SECURITY CLASSIFICATION	
a. Complete Document:	Unclassified
b. Title in Isolation:	Unclassified
c. Summary in Isolation:	Unclassified

3 TITLE

RADIO PHASE MEASUREMENTS VIA ACOUSTO-OPTICS AND A MACH-ZEHNDER INTERFEROMETER

4 PERSONAL AUTHOR(S):

I.G. Fuss

5 DOCUMENT DATE:

October 1984

6 6.1 TOTAL NUMBER OF PAGES: 22

6.2 NUMBER OF REFERENCES: 8

7 7.1 CORPORATE AUTHOR(S):

Electronics Research Laboratory

7.2 DOCUMENT SERIES AND NUMBER

Electronics Research Laboratory 0319-TR

8 REFERENCE NUMBERS

a. Task: DST 82/126

b. Sponsoring Agency:

9 COST CODE:

312452/134

10 IMPRINT (Publishing organisation)

Defence Research Centre Salisbury

11 COMPUTER PROGRAM(S) (Title(s) and language(s))

12 RELEASE LIMITATIONS (of the document):

Approved for Public Release

Security classification of this page: UNCLASSIFIED

Security classification of this page: UNCLASSIFIED

13 ANNOUNCEMENT LIMITATIONS (of the information on these pages):

No limitations

14 DESCRIPTORS:

a. EJC Thesaurus Terms: Radio signals; Acousto-optics

b. Non-Thesaurus Terms: Frequency spectrum; Radio phase measurement

15 COSATI CODES:

17020

16 SUMMARY OR ABSTRACT:
(if this is security classified, the announcement of this report will be similarly classified)

A method for simultaneously measuring the frequency spectra of two radio signals, and their relative phase as a function of frequency is described. Measurements made using a prototype verify aspects of this method.

Security classification of this page: UNCLASSIFIED

The official documents produced by the Laboratories of the Defence Research Centre Salisbury are issued in one of five categories: Reports, Technical Reports, Technical Memoranda, Manuals and Specifications. The purpose of the latter two categories is self-evident, with the other three categories being used for the following purposes:

Reports	:	documents prepared for managerial purposes.
Technical Reports	:	records of scientific and technical work of a permanent value intended for other scientists and technologists working in the field.
Technical Memoranda	:	intended primarily for disseminating information within the DSTO. They are usually tentative in nature and reflect the personal views of the author.

END
FILMED
4-86
DTIC